Ahmad Hajivand
S. Hossein Mousavizadegan
Mohsen Sadeghian
Manochehr Fadavi

http://dx.doi.org/10.21278/brod67102

ISSN 0007-215X
eISSN 1845-5859

EFFECT OF HYDROPLANE PROFILE ON HYDRODYNAMIC COEFFICIENTS OF AN AUTONOMOUS UNDERWATER VEHICLE

UDC 629.5.58:629.572:629.5.015.2
Original scientific paper

Summary

AUVs are the most suitable tool for conduction survey concerning with global environmental problems. AUVs maneuverability should be carefully checked so as to improve energy efficiency of the vehicle and avoid unexpected motion. Oblique towing test (OTT) is simulated virtually in a computational fluid dynamic (CFD) environment to obtain hydrodynamic damping coefficients of a full-scale autonomous underwater vehicle. Simulations are performed for bare hull and hull equipped with four different hydroplanes. The hydrodynamic forces and moment are obtained to calculate hydrodynamic coefficients. Nonlinear damping coefficients are also obtained by using suitable curve fitting. Experiments of resistance and OTT are carried out in specific condition, for validation purpose. Following the extracting numerical results a mathematical model is developed to calculate hydrodynamic force for different sail type in order to predict autonomous underwater vehicle (AUV) maneuverability. The results shows good agreement between theory and experiment.

Key words: *AUV; hydrodynamic coefficient; hydroplane; CFD, maneuver*

1. Introduction

The energy of an AUV is usually supplied by inboard batteries that are certainly limited. Consequently, through the AUV preliminary design stage, the estimation of its maneuverability and controllability is important because it has direct influence on economy and safety. Maneuvering of a marine vehicle is judged based on its course keeping, course changing and speed changing abilities. The regulation bodies and international marine organizations such as IMO recommend criteria to investigate marine vehicles maneuvering quality [1-2].

Maneuverability of a marine vehicle may be predicted by model tests, mathematical models or both. Mathematical models for prediction of marine vehicle maneuverability may be divided into two main categories called as hydrodynamic models, and response models. The hydrodynamic models are of two types and recognized as the Abkowitz [3] and MMG [4]

models. The Abkowitz model is based on the Taylor series expansion of hydrodynamic forces and moments about suitable initial conditions. The MMG model, also called as modular model, decomposes hydrodynamic forces and moments into three components namely: the bare hull; rudder; and propeller and also considers the interaction among the three. The response model investigates the relationship for the motion responses of the vehicle to the rudder action and used to investigate the course control problems [5]

The hydrodynamic models, especially the Abkowitz formulation, are more suitable for computer simulation. It contains several derivatives that are known as the hydrodynamic coefficients. These hydrodynamic coefficients namely added mass and damping coefficients should be determined in advance to proceed into the predicting the maneuvering characteristics of a marine vehicle. All the coefficients are function of the geometry of the vessel but the added mass coefficients depend on the acceleration of the vessel while the damping coefficients are velocity dependent. The added mass coefficients can be computed through the solution of the non-viscous fluid flow around the vessel. The damping coefficients are due to the wave formation in the free surface of the water and the effect of the viscosity. The total damping coefficients may be obtained through the solution of viscous fluid flow around the vessel.

There are several methods to obtain hydrodynamic coefficients such as theoretical approach, semi empirical formulas, captive model tests, and CFD. Theoretical approach is limited to slender bodies and do not consider the interaction between the hull and the appendages. It can provide the added mass coefficients and the part of damping coefficients due to the wave formation on the free surface of water. Semi empirical formulas are obtained using linear regression analysis of captive model test data. They can only provide the linear coefficients for some specific geometrical shape and are inaccurate when the particulars of vessel are outside of the database. The captive model tests provide the hydrodynamic coefficients through the running the tests: rotating arm test (RAT) or circular motion test (CMT) and planar motion mechanism (PMM) test. The planar motion mechanism tests are done in a towing tank and RAT is run in a maneuvering basin. The rotating arm tests (RAT) give the angular velocity dependent coefficients.

The planar motion mechanism tests may be done in a straight path when the model has a drift angle with the fluid flow. Such a test is called as oblique towing-tank test (OTT) and provides the damping coefficients depend on the translational velocities. The oblique towing test is also called as static test since the model is running with a constant velocity in a straight path and therefore, there is no acceleration involve. The planar motion mechanism may also be done in a sinusoidal path with various orientation of the body. These types of tests are also called as dynamic tests since the body is acted by inertia forces. These types of model tests need special equipment and are expensive, time consuming and their results include the scaling effects due to inconsistency of Reynolds number between the vessel and the model.

CFD can also be used to obtain the maneuvering hydrodynamic coefficients of a marine vehicle by virtual simulation of the captive model tests. CFD methods are used the Navier Stokes equations to model a given fluid flow. There are various approaches to solve the fluid flow equation for a viscous flow such as the flow around a maneuvering AUV. These methods may be listed as direct numerical simulation (DNS), large eddy simulation (LES) and Reynolds averaged Navier Stokes (RANS) methods. DNS and LES need very high computational capacity. RANS models are time-averaged formulations of fluid flow motion equations and are based on statistical tool known as Reynolds decomposition.

Application of RANS to solve the maritime problems goes back to [6] and [7] who obtained unsatisfied results. By increasing of computing capacities and recent progress in RANS models, stunning advances in this field are achieved. Nowadays, CFD is crucial tool for

various aspect of a marine vehicle hydrodynamics not only for research but also as a design tool. One of the most recently and important application of CFD in marine industry is computation of hydrodynamic coefficients of marine vehicles by simulating the captive model tests. Sarkar et al. [8] develop a new computationally efficient technique to simulate the 2-D flow over axisymmetric AUVs by Using the PHOENICS CFD package. Nazir and Wang [9] and Zhang, and Cai [10] apply the Fluent CFD code to obtain hydrodynamic coefficients of 3-D fins and an AUV, respectively. Tyagi and Sen [11] compute transverse hydrodynamic coefficients of an AUV using a commercial CFD package. The hydrodynamic forces and moments on an AUV due to the deflection of control surfaces are investigated using ANSYS Fluent software by Dantas and DeBarros [12].
Ray et al. [13] applies Fluent code to compute linear and nonlinear hydrodynamic coefficients of the SUBOFF submarine in an unrestricted fluid flow. Jagadeesh et al. [14] study the forces and moment on AUV hull form in the vertical plane by doing experimental tests and also using CFD. Phillips et al. [15] using CFD to investigate the influence of turbulence closure models on the vertical flow field around a DOR submarine body undergoing steady drift and cost-effective hydrodynamic design of autonomous underwater vehicles.
The Star-CCM+ CFD package is applied to simulate the oblique towing tests (OTT) for a Myring AUV. The simulations are performed for five configurations: bare hull and hull equipped with four different hydroplanes. The OTT simulations are done for wide range of the drift angles to obtain linear and nonlinear damping coefficients. The realizable k-ε model is used to consider the turbulent effects. Grid convergence is performed for simulations. Furthermore Experiments of resistance and OTT tests are carried out in specific condition in the towing tank of Isfahan University of Technology for validation purpose. It is found that the results of simulations comply with the experimental data.

2. Description of the model

The Myring model type of AUV is chosen due to its keeping streamlined characteristics. The Myring AUV class has already applied in the aircraft's fuselage and other AUV's such as Maya and Remus, and Pirajuba, Guanay II. A Myring type AUV has three distinct parts, the bow section, the middle body cylindrical section, and the stern section. The bow and the stern sections are defined by the semi-elliptical radius distribution along the main axis as given by the following equations (Myring, 1974):

Bow:

$$r(x) = \frac{1}{2} d \left[1 - \left(\frac{x-a}{a} \right)^2 \right]^{1/n} \tag{1}$$

Stern:

$$r(x) = \frac{1}{2} d - \left[\frac{3d}{2c^2} - \frac{\tan\theta}{c} \right] (x-a-b)^2 + \left[\frac{d}{c^3} - \frac{\tan\theta}{c^2} \right] (x-a-b)^3 \tag{2}$$

Where d is the maximum diameter of the body, a is the bow length of the body, b is the middle body length of the body, c is the stern length of the body, l is the overall length, n is the Myring parameter and θ is tail semi angle. The middle part is a cylinder with constant diameter d. The dimensions of the model are given in Fig. 1 and table 1.

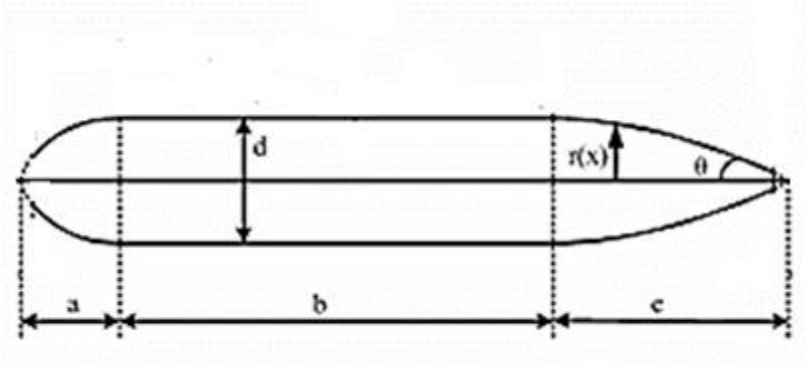

Fig.1 The geometry of a Myring AUV

Table1: The dimensions of the AUV model		
Hull Maximum Diameter(d)	0.234	m
Stern Length(c)	0.279	m
Bow Length(a)	0.217	m
Middle Body Length(b)	1.246	m
Tail semi-angle(θ)	25	Deg
Myring Body Parameter	2	-

To investigate the effect of hydroplane profile on hydrodynamic characteristics, four all moveable control surfaces with the section NACA0012, NACA0015, NACA0018, NACA0020 are considered. The hydroplanes are shown in Fig. 2. The dimension of hydroplanes are presented in table 2.

Fig.2 Four different NACA hydroplanes that installed on bare hull

3. Experimental Setup

Towing resistance and OTT are done in certain conditions for validation of numerical results. Experiments are conducted in the towing tank of Isfahan University of Technology ($108\times3\times2.2$m). The basin is equipped with a trolley that can provide carriage speed up to 6m/s with ±0.02 m/s accuracy. For force measurements a 3-DOF dynamometer is installed with 100 N load cells that is calibrated by calibration weights with 1% uncertainty.

The resistance test at various forward speeds (U=0.5, 0.75, 1, 1.5 and 2m/s) are done due to limitation in the towing tank. The tests are done in five configurations, bare hull and hull equipped with four different hydroplanes. The results of tests are given in CFD section to compare and validate numerical computations. The experimental set up are shown in Fig .3.

Table2: The dimensions of hydroplanes				
	NACA0012	NACA0015	NACA0018	NACA0020
Mean chord(m)	0.137	0.148	0.156	0.183
Mean span(m)	0.063	0.082	0.089	0.095

Fig.3 Experimental setup

4. Maneuvering Equation

A body coordinate system o-xyz (Fig. 4) is defined so that oz is vertical axis and positive downward, ox is the longitudinal axis and positive toward the bow of the vehicle and oy is the lateral axis and positive toward the starboard side of a vehicle. If it is assumed the body is moving in horizontal plane o-*xy*, the origin o coincide with the center of mass and the coordinate system coincide with the principle axes of inertia. The motion equation may be given as follows for an AUV in the body coordinate system o-xyz that is moving relative to inertial coordinate system $o\text{-}x_E y_E z_E$

$$m(\dot{u} - rv) = X \tag{3}$$

$$m(\dot{v} + ru) = Y \tag{4}$$

$$I_z \dot{r} = N \tag{5}$$

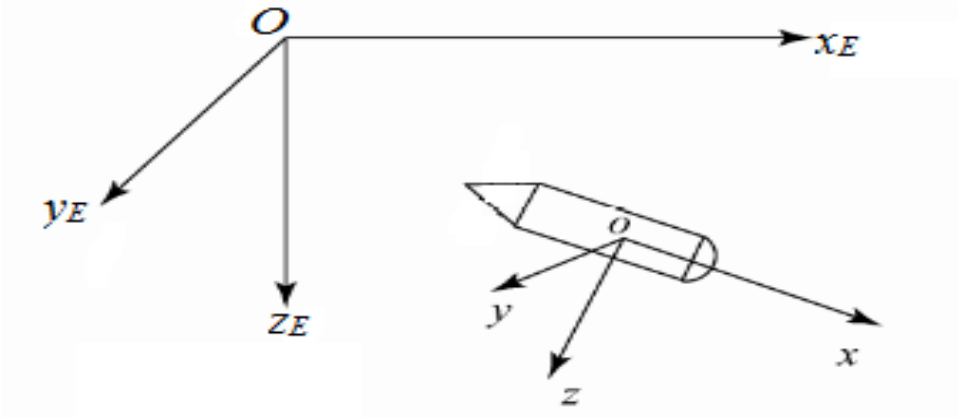

Fig. 4 Earth-fixed and body-fixed coordinate system

These equations are surge, sway, and yaw motion equations, respectively. The notation m is the mass of the body, Iz is the moment of inertia of the body about z-axis, u and v are the velocity of the body along x and y directions, respectively. The notations $\dot{u}$ and $\dot{v}$ are the acceleration of the body along x and y directions, respectively, and r and $\dot{r}$ are the angular velocity and acceleration around the z-axis of the body. The notations X and Y are external forces along x and y axis, respectively and N is the external moment about the z-axis.

The external forces X and Y and moment N may be written as follows according to the Abkowitz model with the assumption that the body is moving in self-propulsion point and the control surface are in neutral condition.

$$\begin{aligned} X &= X_{\dot{u}}\dot{u} + X_u u + X_{uu}u^2 \\ &+ X_{vv}v^2 + X_{rr}r^2 + X_{vvu}v^2u \\ &+ X_{rru}r^2u + {}_{vr}\, vr + X_{vru}vru \end{aligned} \tag{6}$$

$$\begin{aligned} Y &= Y_{\dot{v}}\dot{v} + Y_{\dot{r}}\dot{r} + Y_v v + Y_{vvv}v^3 \\ &+ Y_{vrr}vr^2 + Y_{vu}vu + Y_{vuu}vu^2 + Y_r r \\ &+ Y_{rrr}r^3 + Y_{rvv}rv^2 + Y_{ru}ru + Y_{ruu}ru^2 \end{aligned} \tag{7}$$

$$\begin{aligned} N &= N_{\dot{v}}\dot{v} + N_{\dot{r}}\dot{r} + N_v v + N_{vvv}v^3 \\ &+ N_{vrr}vr^2 + N_{vu}vu + N_{vuu}vu^2 + N_r r \\ &+ N_{rrr}r^3 + N_{rvv}rv^2 + N_{ru}ru + N_{ruu}ru^2 \end{aligned} \tag{8}$$

Where the notations such as X_u , Y_v and etc, are hydrodynamic derivatives with respect to the motion variables such as u, v, r and etc. These derivatives are also called maneuvering coefficients. The PMM tests are usually used to obtain all these coefficients that are known as damping and added mass coefficients. There different types of PMM tests that are all done in a towing tank. One of them are oblique towing tank (OTT) test that the body is towing with a drift angle. The OTT is simulated in CFD to obtain the transverse velocity dependent coefficient Y_v , N_v, X_{vv}, Y_{vvv} and N_{vvv}, .

5. Fluid Flow Modelling

The unsteady viscous flow around a marine vehicle is governed by the Navier Stokes equations. Navier-Stokes equations can be applied to both laminar and turbulent flow but a very fine meshing is necessary to capture all the turbulence effects in a turbulent flow regime. RANS equations can also be applied to model the turbulent flow. The RANS equations are obtained based on statistical tools known as Reynolds decomposition where the flow parameters are decomposed into time-averaged and fluctuation parts, i.e. $u = \bar{u} + u'$, $p = \bar{p} + p'$ where $\bar{u}, \bar{p}$ are the time-averaged and u', p' are the fluctuation velocity and pressure, respectively. The RANS equations may be given as follows for an incompressible flow [16].

$$\frac{\partial(\rho\bar{u}_i)}{\partial t} + \frac{\partial}{\partial x_j}(\rho\bar{u}_i\bar{u}_j + \rho\overline{u_i'u_j'}) = -\frac{\partial\bar{p}}{\partial x_i} + \rho g_i + \frac{\partial}{\partial x_j}\left(\mu\left(\frac{\partial\bar{u}_i}{\partial x_j} + \frac{\partial\bar{u}_j}{\partial x_i}\right)\right) \tag{9}$$

$$\frac{\partial(\rho\bar{u}_i)}{\partial x_i} = 0 \tag{10}$$

Where ρ is the fluid density, g_i is the x-, y- and z- components of gravitational acceleration, and μ is fluid dynamic viscosity. $\rho\overline{u_i'u_j'}$ is the Reynolds stress tensor components. The Reynolds stress tensor components are estimated by turbulence models which are approximations to the physical phenomena of turbulence.

. The realizable k-ε is used to model the turbulence effects. In this model the effect of Reynolds stresses is considered as an additional eddy viscosity which is a property of the flow. Eddy viscosity expressed as:

$$\mu_t = \rho C_\mu \frac{k^2}{\varepsilon} \tag{11}$$

Where *k* is the turbulence kinetic energy per unit mass, ε is the rate of the dissipation of the turbulence kinetic energy per unit mass. and C_μ is a dimensionless quantity that is expressed as a function of mean flow and turbulent properties [16]. The turbulent kinetic energy and the dissipation rate are calculated from the solution of transport equations. Rather than standard k- ε model realizable k- ε calculate the turbulent dissipation rate ε by solving a new transport equation that is based on the dynamic equation of the mean-square vorticity fluctuation [17].

5.1. MESH GENERATION

Finite volume method (FVM) is the common approach to solve RANS equations in computational domain. The computational domain is discretized to finite control volumes and discretized RANS equations are solved within them. Domain dimensions are selected sufficient large to avoid back flow at high drift angles. Distance of the inlet and outlet boundary from AUV center is considered 1.5*l*. The side boundaries are located at 1.25*l*and the top and bottom boundary is located at 0.75*l* from AUV centerline (Fig. 5).

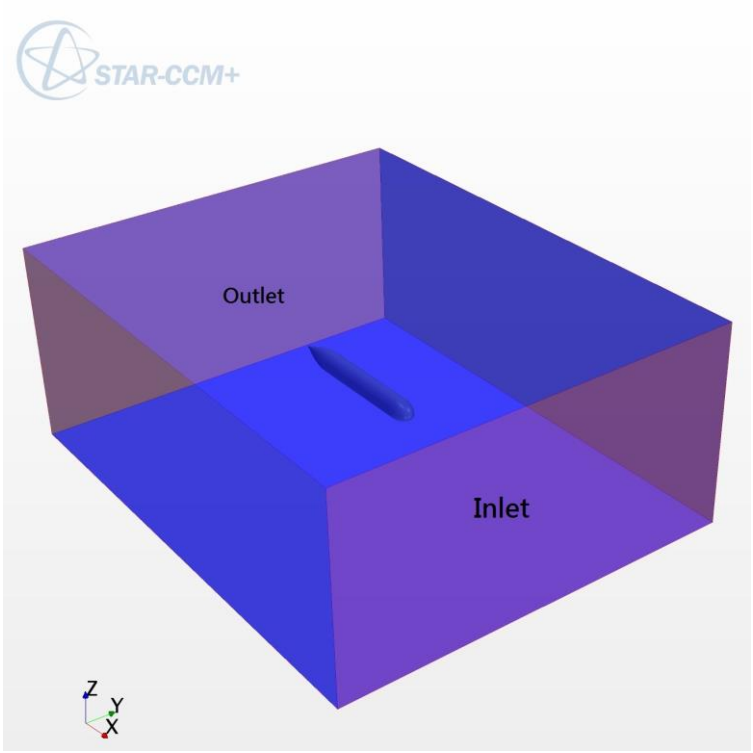

Fig. 5 Illustration of computational domain.

There are different structured and unstructured meshing strategies to solve various problems. Simulation are conducted on unstructured trimmed meshes. The trimmer meshing strategy is a proficient and strong method that generates high quality mesh with lowest grid skewness. The overall view of the mesh in computational domain and around the AUV is displayed in Figs. 6 and 7, respectively.

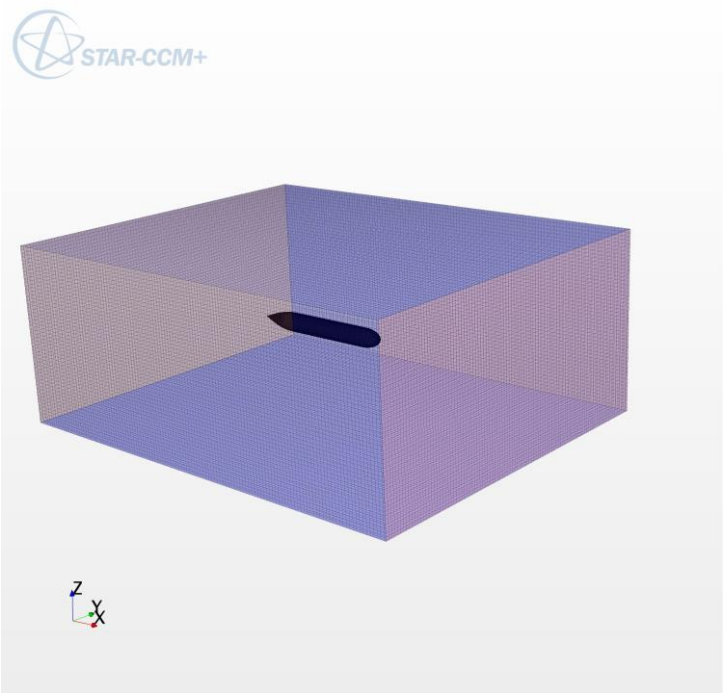

Fig 6.Discretd Computational domain.

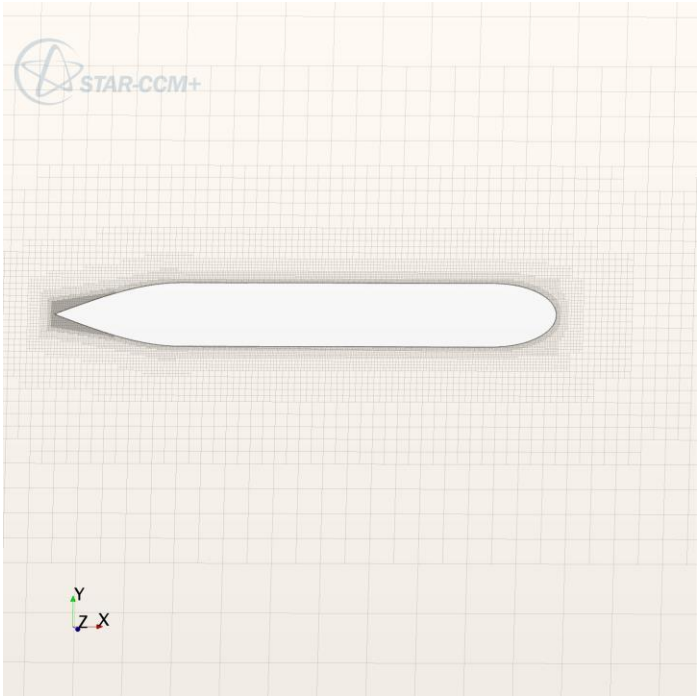

Fig 7. Mesh around hull

Prism layer refinement is applied around the hull to improve the accuracy of the solution in the boundary layer region. The turbulent flow inside the boundary layer is approximated by wall functions. High y^+ wall treatment that is based on equilibrium turbulent boundary layer theory is used as wall function approach. The mean value of y^+ on the hull surface is around 30 that show refinement of prism layer is well. Distribution of y+ for fine mesh on hull is shown in Fig. 8.

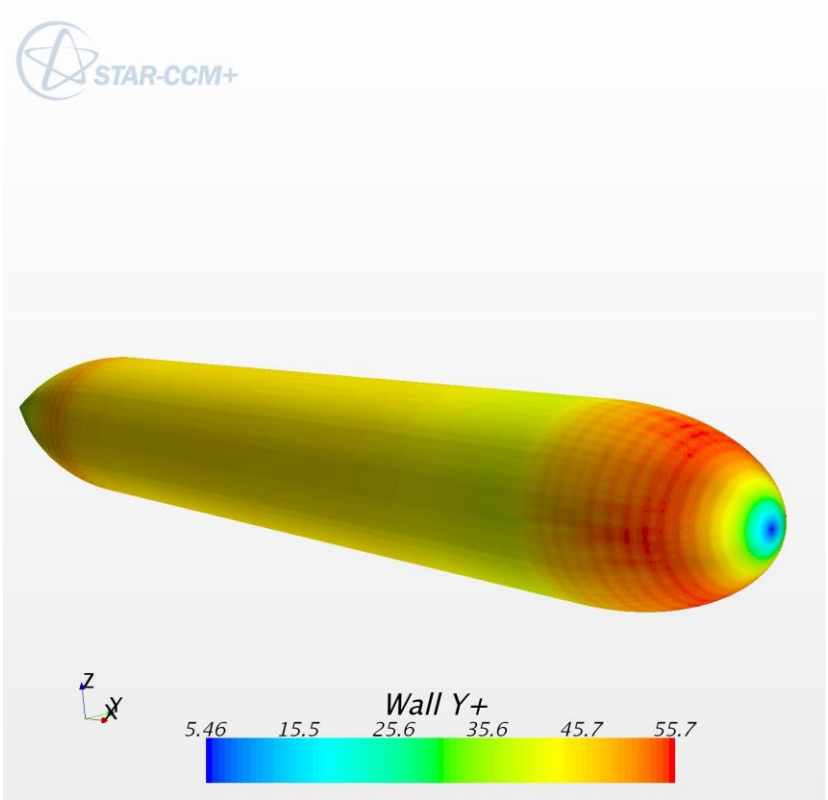

Fig 8. Distribution of y^+ around hull

5.2. Boundary Conditions

Appropriate boundary conditions on the fluid domain boundaries and AUV's hull must be applied to create a well-posed system of equations. The boundaries of domain split into patches as shown in Figure 5. The boundary conditions are chosen such that to avoid back flow and lateral wall effects. For body surface there are two boundary conditions. The first is the kinematic condition of no flow through the surface. And the second is a no slip condition on the tangential velocity. These are applied on the instantaneous wetted surface of the AUV. For other boundaries the symmetry plane condition is a Neumann condition which means pressure, tangential velocities and turbulence quantities have a zero gradient normal to the surface but for the normal velocity component, a Dirichlet condition, is applied.

5.3. Grid Convergence

Mesh sensitivity examination is the most straight-forward and most consistent technique for determining the order of discretization error in numerical simulation. In other words, numerical results can be considered as precise and valid if its solution be independence of the grid. A mesh sensitivity study comprises implementation solution on the CFD model, with sequentially refined grids of reduced mesh size, until the variables become independent of the mesh size. Three different mesh sizes with constant grid refinement factor, $r = h_2 / h_1 = h_3 / h_2 = 1.65$, have been chosen. h_i is a characteristic dimension of the model, for example AUV length, that use as a measure of the mesh discretization. To avoid the errors arising from extrapolation, based on experiences it is recommended that $r > 1.3$. Corresponding solution for these cases are designated s_1 through s_3.

Mesh study for simulations are examined for the pure drift condition with 9 degrees drift at U=2m/s.

The corresponding forces and moment for each meshes are calculated. Mesh numbers and forces and moment are shown in table3.

Table3: Forces and moment for different grid

Number of grid points	F_x(N)	F_y(N)	M_z(N.m)
1,456,325	-11.871	10.725	18.620
2,529,846	-10.620	9.582	19.461
4,077,078	-10.362	9.348	19.853

Convergence ratio defined as follows.

$$R = \frac{\varepsilon_{21}}{\varepsilon_{32}}$$

Where

$\varepsilon_{21} = s_2 - s_1$ is difference between solution of fine and medium grid

$\varepsilon_{32} = s_3 - s_2$ is difference between solution of medium and coarse grid

The possible convergence situations are:

$R > 1$: Grid divergence

$R < 0$: Oscillatory convergence

$0 < R < 1$: Monotonic Grid convergence

If grid convergence occurs, Richardson extrapolation also called h^2 extrapolation is used to estimate convergence rate. Fractional difference between solutions defined as $e_{ij} = (s_j - s_i)/s_i$, hence order of discretization estimated as follows:

$$p = \frac{\log(e_{32}/e_{21})}{\log(r)} \tag{12}$$

After that Grid Convergence Index (GCI) is defined

$$GCI_{ij} = F_S \frac{|e_{ij}|}{r^p - 1} \tag{13}$$

In this equation F_S is a safety factor that Roache [18] recommended for convergence studied with minimum three grids $F_S = 1.25$. GCI indicates the difference between calculated and exact value. On the other hand, GCI is a measure of solution changes with more grid refinement. Small value of GCI means that the solution is in exact value range.

Computed Convergence ratio, order of discretization and GCI are shown in table 4. Theoretical value for convergence is p=2. The difference is due to grid orthogonally, problem nonlinearities, turbulence modelling and etc.

Table 4. Estimated convergence ratio, order of discretization and GCI

	F_x	F_y	M_z
R	0.206	0.205	0.466
p	2.930	2.942	1.613
GCI_{fine}	0.009	0.009	0.020

6. COMPUTATIONAL FLUID DYNAMIC SIMULATIONS

The fluid flow around Myring model is simulated with and without drift angle with respect to the fluid flow direction. For the case without drift angle, the resistance can be obtained. This is called as resistance simulation. For the case with drift angle which is called as static drift angle the lateral velocity dependent damping coefficients can be obtained. All computation are done with SIMPLE algorithm for pressure-velocity coupling. The second-order upwind scheme is applied for advection term in momentum equation. The most common way to check the convergence of the simulation results is to investigate the residual of each variable that being solved. In Fig. 9 an illustrated of residual is shown that indicated good convergence.

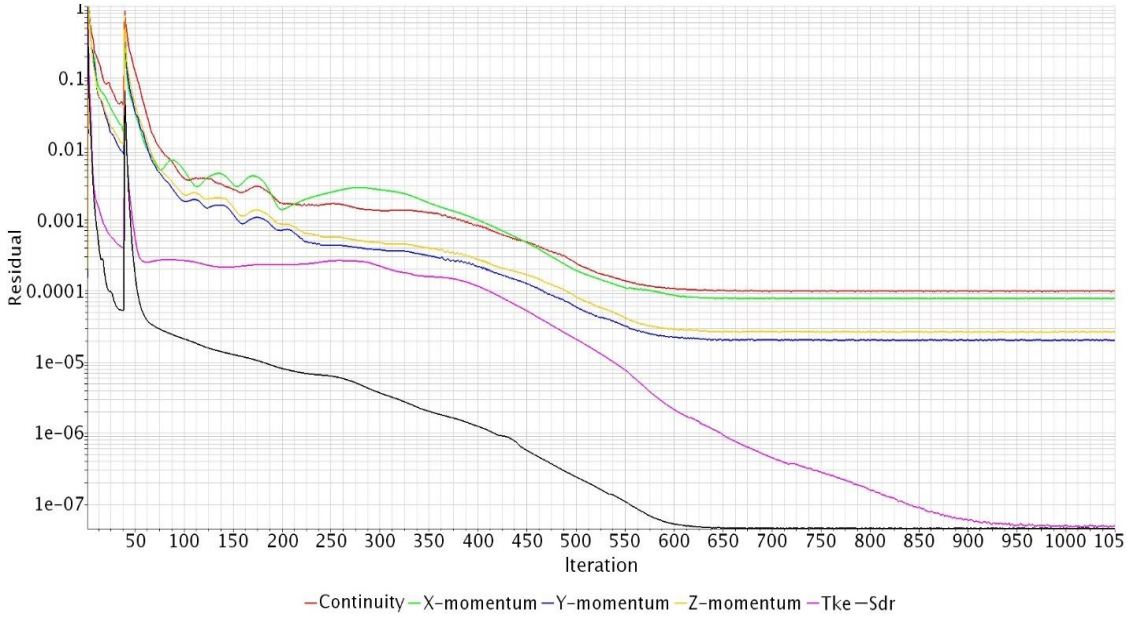

Fig. 9 Residual of continuity, momentum and turbulence parameters

6.1. Resistance simulation

The resistance test is simulated for bare hull and appended hull at U=0.5-2.5m/s with an increment of 0.5m/s to investigate the effect of hydroplane profile on AUV resistance characteristics. Furthermore resistance of the bare hull is estimated based on the empirical algorithm proposed by Hoerner. In this method the resistance is predicted as

$$R_{BH} = \frac{1}{2}\rho A V^2 C_t \tag{14}$$

Where A is the wetted surface area, V is velocity, ρ is water density and C_t is total drag coefficient of the hull and calculated as follow

$$C_t = C_f \left[1+1.5\left(\frac{d}{l}\right)^{1.5} + 7\left(\frac{d}{l}\right)^{3}\right] \tag{15}$$

Where C_f is frictional resistance coefficient that is calculated according to ITTC 1957 friction formula

$$C_f = \frac{0.075}{\left(\log_{10} R_e - 2\right)^2} \tag{16}$$

Where R_e is Reynolds number. In Fig. 10 the results obtained for bare hull resistance are shown. Experimental and empirical results are presented for comparison. The data points and quadratic polynomial fitted curves, $R=aV^2$, are included in figure. It can be seen that the CFD solution provides good prediction with an error up to 11% and 14% with empirical and experimental results, respectively, for different velocities. In table 5 curve fitting parameters including curve coefficient, a, and goodness of fit parameter, R_{square} are presented.

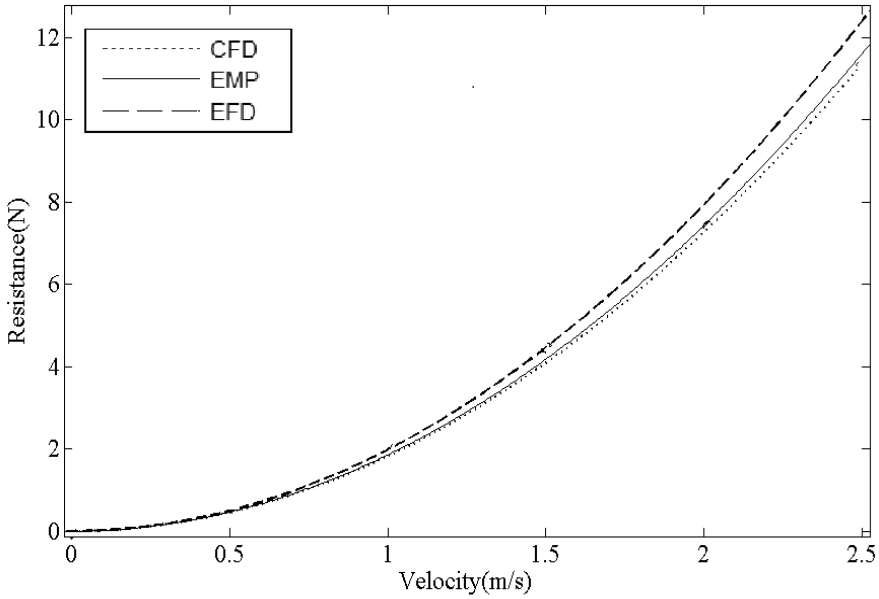

Fig. 10 Compare computed, experimental and empirical resistance vs. velocity

Table 5. Curve fitting parameters for resistance results

	CFD	EFD	EMP
a	1.815	1.982	1.858
R_{square}	0.986	0.945	0.996

In table 6 the obtained results for resistance of bare hull and appended hulls are compared for U=1-2.5m/s with an increment of 0.5m/s. it can be seen resistance of an appended hull is higher than a bare hull between 3-10% for different speeds. However, by increasing the thickness of the hydroplane the total drag slightly increased up to 0.6%.

Table 6. Resistance of bare hull and appended hull

U(m/s)	R(bare) (N)	R(Naca0012)(N)	R(Naca0015)(N)	R(Naca0018)(N)	R(Naca0020)(N)
1.0	2.029	2.250	2.259	2.271	2.282
1.5	4.566	4.736	4.756	4.781	4.802
2.0	7.651	8.085	8.098	8.124	8.168
2.5	10.684	11.166	11.218	11.285	11.338

6.2. OTT simulation

The OTT is simulated in CFD to evaluate the linear and nonlinear velocity dependent damping coefficients. The OTT is done with a constant inflow speed of V at various drift angles β. A right handed coordinate system fixed to the body is defined so that $x-$ and $y-$ axis are longitudinal and transverse axes as depicted in Fig. 4. The $z-$ axis is the vertical axis and positive downward. The components of the flow velocity along the $x-$ and $y-$ axis are $u=-V\cos\beta$ and $v=-V\sin\beta$. The body is acted by a hydrodynamic force with components X and Y along the longitudinal and transverse axes respectively. The body is

also acted by a moment N about the vertical axis z . If the initial condition is defined when the drift angle β is zero and considering the symmetry about *xz* plane, the components of hydrodynamic force and moment may be given as follows using Taylor series expansion.

$$X = X_0 + X_{vv}v^2 \tag{17}$$

$$Y = Y_v v + Y_{vvv}v^3 \tag{18}$$

$$N = N_v v + N_{vvv}v^3 \tag{19}$$

Where $X_{vv}, Y_v, Y_{vvv}, N_v$ and N_{vvv} are transverse velocity dependent damping coefficients. The coefficients Y_v and N_v are the linear coefficients and the rest are nonlinear ones. Simulation of OTT at various drift angle β provides the forces X and Y and moment N . By using a curve fitting to the data of forces and moment as a function of β , the hydrodynamic derivatives or coefficients $X_{vv}, Y_v, Y_{vvv}, N_v$ and N_{vvv} are obtained.

The simulation of OTT on CFD environment with is done at drift angle $\beta = \pm 0, 2, 6, 9, 10, 11, 12, 16, 20$ degrees with $V = 2m/s$ for the bare hull and the hull appended with different hydroplanes.

Velocity distribution around the AUV hull equipped with NACA0018 for $\beta = 0,\ 6, 12,\ 20$ degrees are shown in Figs.11-14, at *V*=2m/s. it can be seen that by increasing the drift angle the maximum velocity increased. Pressure distribution around different hydroplane for $\beta = 9°$ at V=2m/s are shown in Figs. 15-18. This figures show that by decreasing the hydroplane thickness maximum pressure on hydroplane stagnation point slightly increased.

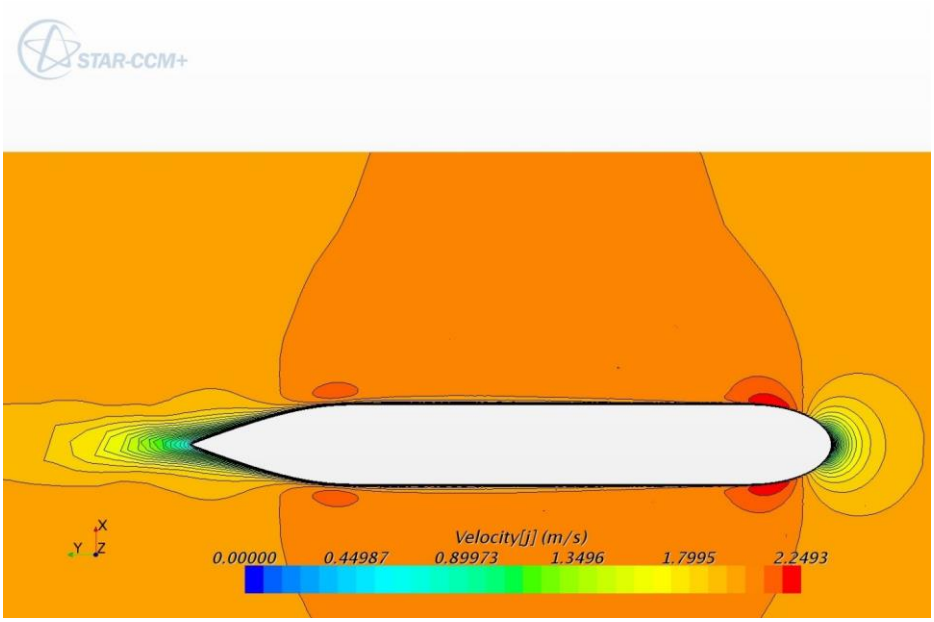

Fig. 11 Velocity distribution around hull for $\beta = 0°$

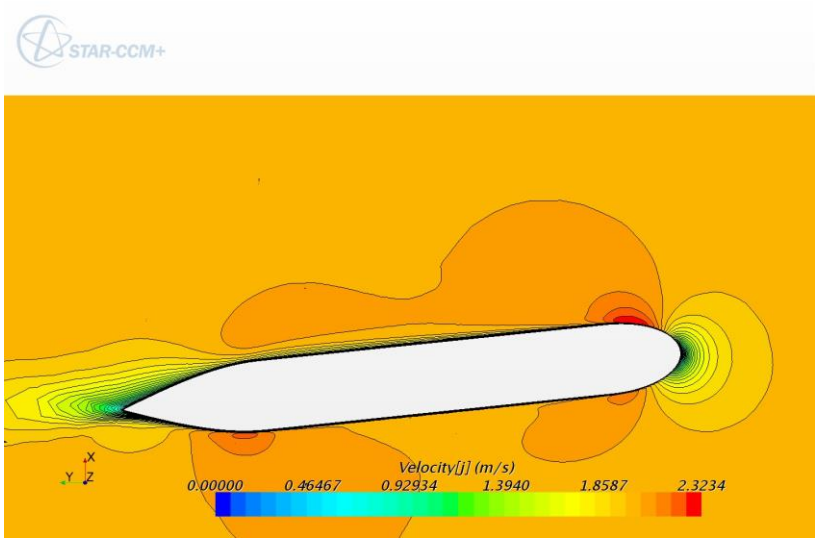

Fig. 12 Velocity distribution around hull for $\beta = 6°$

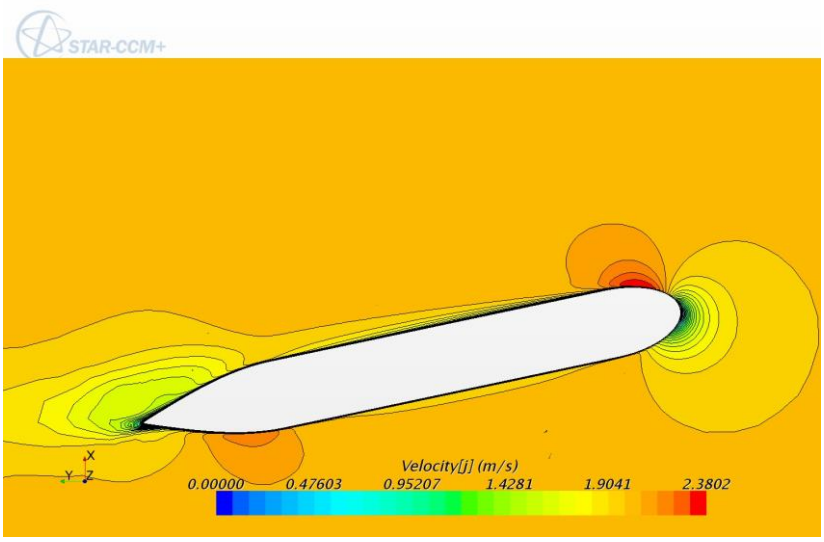

Fig. 13 Velocity distribution around hull for $\beta = 12°$

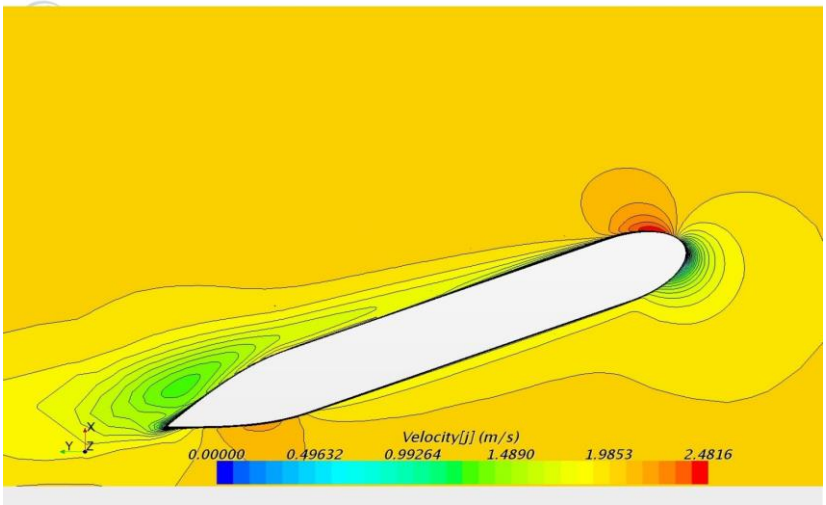

Fig. 14 Velocity distribution around hull for $\beta = 20^{\circ}$

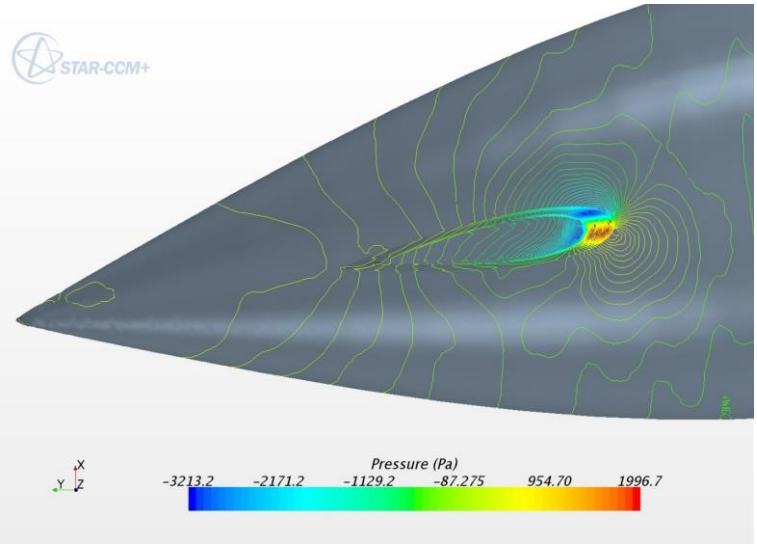

Fig. 15 Pressure distribution around NACA0020 for $\beta = 9°$

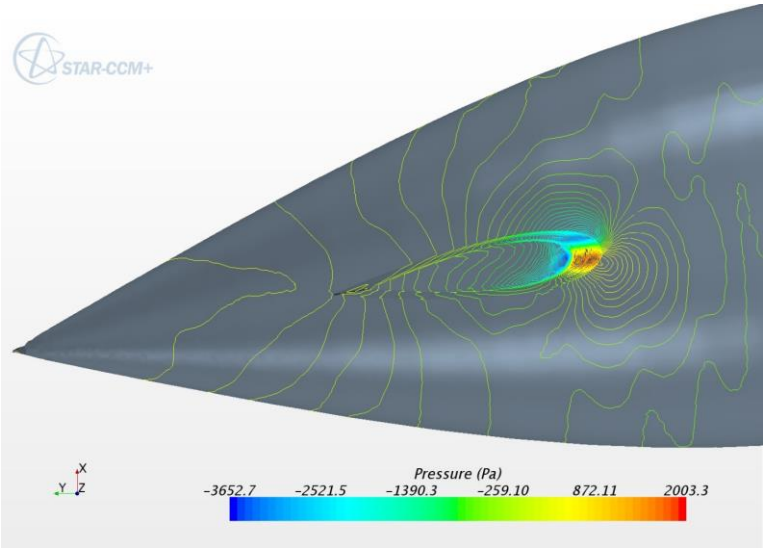

Fig. 16 Pressure distribution around NACA0018 for $\beta = 9°$

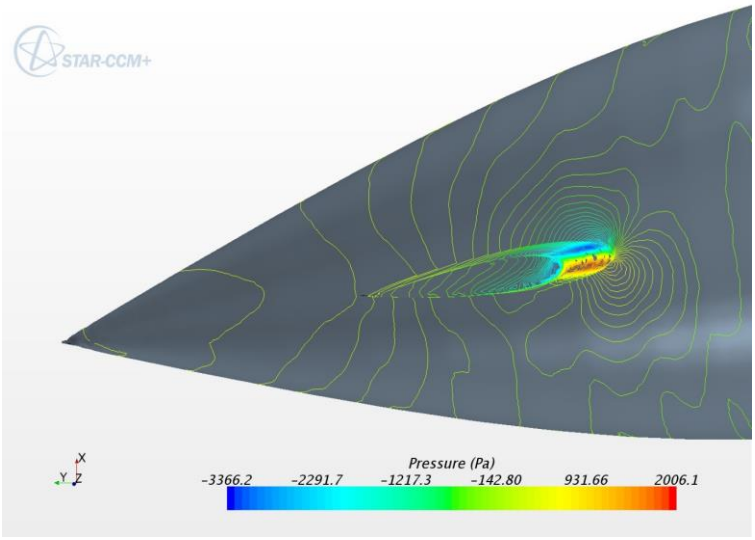

Fig. 17 Pressure distribution around NACA0015 for $\beta = 9°$

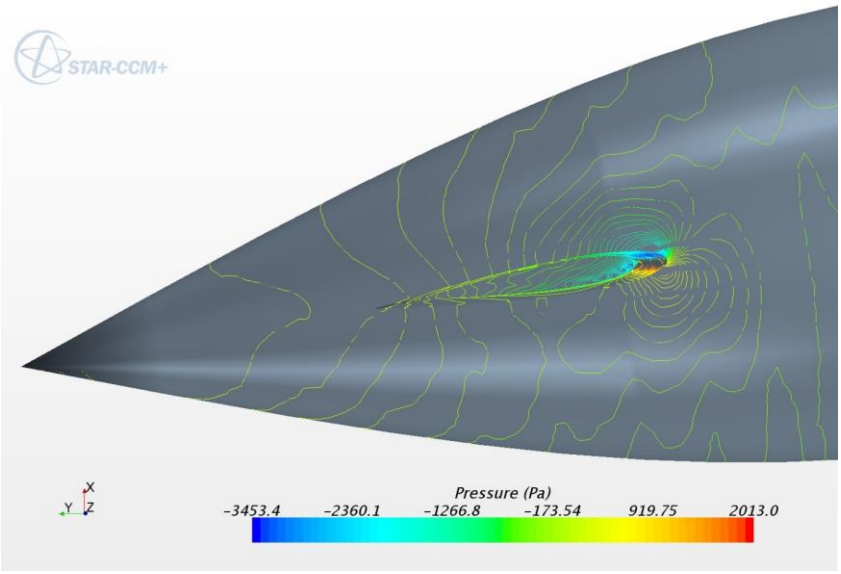

Fig. 18 Pressure distribution around NACA0012 for $\beta = 9°$

Time mean values for longitudinal and transverse forces are shown in Figs. 19 and 20 as a function of drift angle β for *V=2m/s*. Data are fitted to a quadratic and cubic polynomial.

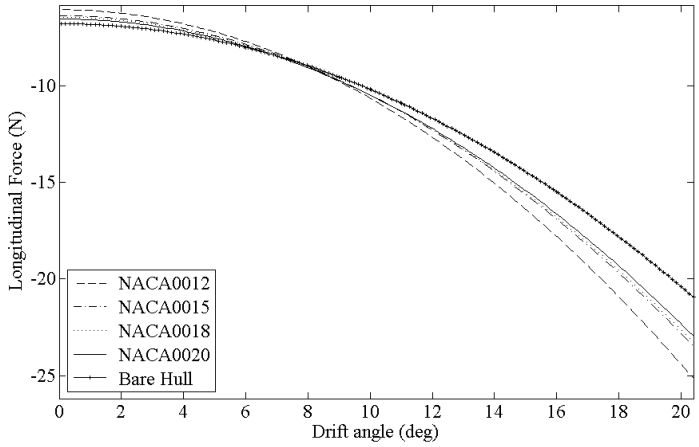

Fig. 19 Longitudinal force vs. drift angle for bare hull and appended hulls

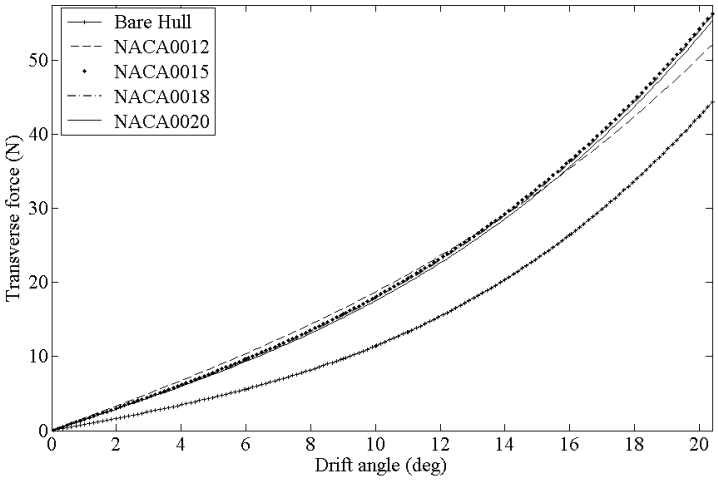

Fig. 20 Transverse force vs. drift angle for bare hull and appended hulls

The solutions for longitudinal force should be symmetrically about $\beta = 0$ for identical drift angle to port or to starboard due to the symmetrical shape of the body. The non-dimensional transverse force should have identical value with different sign for identical drift angle to port and starboard due to the symmetrical shape of the body.

The yaw moment is also depicted in Fig. 21 as a function of β for *V=2m/s*. Data are fitted to a cubic polynomial. The $N-\beta$ graph should demonstrate a symmetrical shape with respect about $\beta = 0$.

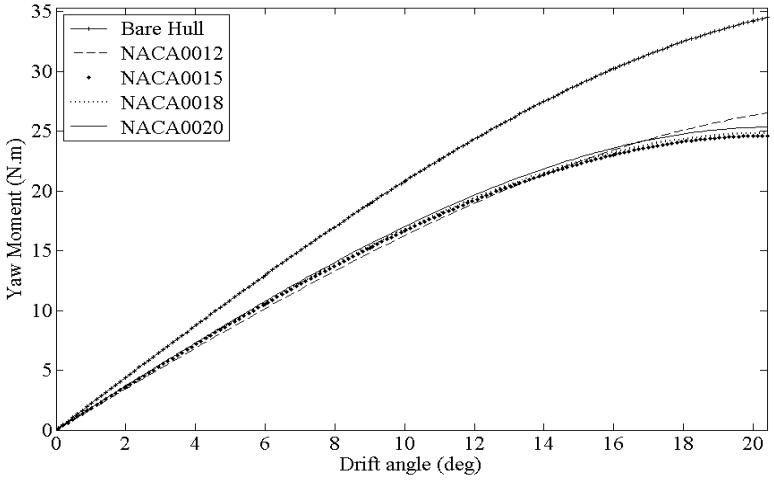

Fig. 21 Yaw moment vs. drift angle for bare hull and appended hulls

The derivatives Y_v and N_v can be obtained from the transverse force and yaw moment curves against β from chain rule as follows.

$$Y_v = \left.\frac{\partial Y}{\partial \beta}\right|_{\beta=0} \left.\frac{\partial \beta}{\partial v}\right|_{v=0} = \frac{1}{V} \left.\frac{1}{\sqrt{1-\left(\frac{v}{V}\right)^2}}\right|_{v=0} Y_\beta\Big|_{\beta=0} \tag{20}$$

$$N_v = \left.\frac{\partial N}{\partial \beta}\right|_{\beta=0} \left.\frac{\partial \beta}{\partial v}\right|_{v=0} = \frac{1}{V} Y_\beta\Big|_{\beta=0} \tag{21}$$

The derivatives Y_β and N_β are the slope of the transverse force and yaw moment curves against drift angle at $\beta = 0°$. The values of Y_v and N_v are obtained using (20, 21) and are given in table 7. It can be seen that Y_v is increased by using hydroplane and N_v is decreased relative to bare hull configuration.

Table 7. Linear hydrodynamic for bare hull an appended hull

	Bare Hull	NACA0012	NACA0015	NACA0018	NACA0020
Y_v	22.66	46.85	42.4	41.71	40.88
N_v	63.4	49.79	52.19	52.64	53.14

The nonlinear derivatives, X_{vv} ,Y_{vvv}, and N_{vvv} are obtained from the longitudinal and transverse forces and yaw moment curves against β by using chain rule of differentiation.

$$X_{vv} = \left.\frac{\partial^2 X}{\partial \beta^2}\right|_{\beta=0} \left(\frac{\partial \beta}{\partial v}\right)^2 = \left(\frac{1}{V}\right)^2 X_{\beta\beta}\Big|_{\beta=0} \tag{22}$$

$$Y_{vvv} = \left.\frac{\partial^3 Y}{\partial \beta^3}\right|_{\beta=0} \left(\frac{\partial \beta}{\partial v}\right)^3 = \left(\frac{1}{V}\right)^3 Y_{\beta\beta\beta}\Big|_{\beta=0} \tag{23}$$

$$N_{vvv} = \left.\frac{\partial^3 N}{\partial \beta^3}\right|_{\beta=0} \left(\frac{\partial \beta}{\partial v}\right)^3 = \left(\frac{1}{V}\right)^3 N_{\beta\beta\beta}\Big|_{\beta=0} \tag{24}$$

The nonlinear derivative $X_{\beta\beta}$ is obtained by finding the second derivative of the longitudinal force curve against drift angle at $\beta = 0°$. This can be obtained by using a curve fitting and finding the second derivatives of the fitted curve. The derivatives $Y_{\beta\beta\beta}$ and $N_{\beta\beta\beta}$ are also obtained by calculating the third derivative of the transverse force and yaw moment curves against drift angle at $\beta = 0°$. These are obtained by using curve fittings to the related data. The solutions for these derivatives are given in table 8. The experimental results are also given in these tables for comparison. The differences among the numerical solutions and experimental solutions are more for nonlinear derivatives than the linear ones.

Table 8. Nonlinear hydrodynamic for bare hull an appended hull

	Bare Hull	NACA0012	NACA0015	NACA0018	NACA0020
Y_{vvv}	9.53	13.09	13.025	13.185	13.13
N_{vvv}	-4.751	-4.033	-5.775	-5.806	-5.73
X_{vv}	-29.037	-39.108	-35.087	-34.485	-35.615

From the extracting numerical results, the mathematical model is developed base on the dimensional analysis. To simplify the problem, effects of parameters such as angle of attack and foil dimensional variation have been studied.

$$\delta F = f(d,t,\beta,\rho)$$
$$\delta M = f(d,t,\beta,\rho) \tag{25}$$

By using parameters d, ρ and V two dimensionless groups are obtained using Buckingham p theorem as follows

$$\frac{M}{\rho V^2 d^3}, \frac{F}{\rho V^2 d^2} = \left(\beta, \frac{t}{d}\right)$$

So according to the principle of superposition, the dimensionless interaction force, F_I and moment, M_I, between body and hydroplane derived as follows:

$F_I=F_T-(F_H-F_F)$

$M_I=M_T-(M_H-M_F)$

Where F_T and M_T are force and moment of appended hull, respectively. F_H and M_H are force and moment of bare hull, respectively and F_F and M_F are hydroplane force and moment.

Figs.22-24 show the Interaction forces at different angles of attack using various hydroplanes are presented. The interaction forces and moments between the body and hydroplane are expressed as mathematical equations with a 3-parameters equations using mathematical statistical relationship.

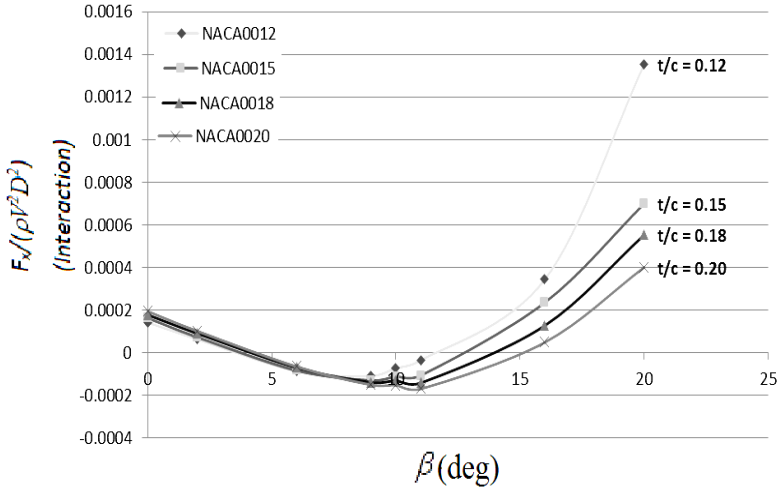

Fig. 22 Non-dimensional longitudinal interaction force vs. drift angle for appended hulls

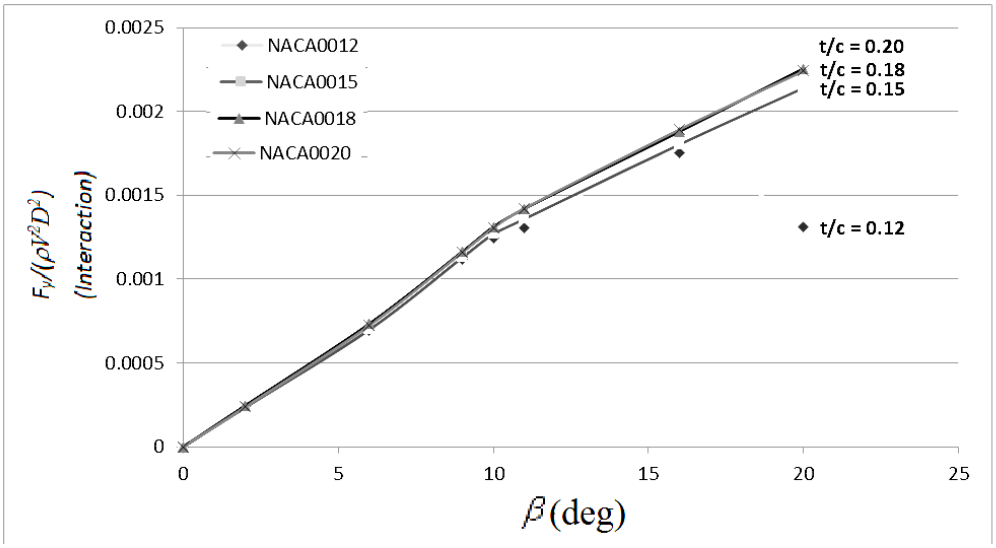

Fig. 23 Non-dimensional transverse interaction force vs. drift angle for appended hulls

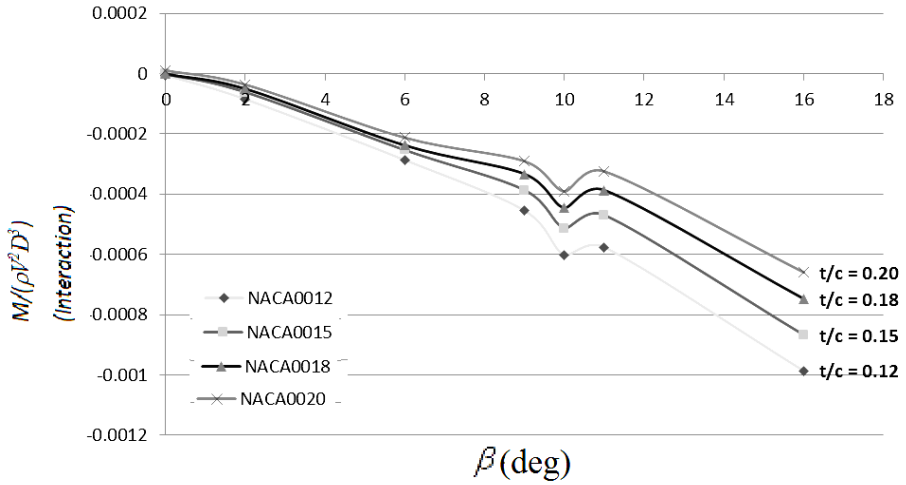

Fig. 24 Non-dimensional yaw interaction moment vs. drift angle for appended hulls

$$F_{Interaction(x)} = 4.873\times10^{-5}\theta - 2.607\times10^{-5}Z_1\theta - 3.466\times10^{-5}Z_2\theta - 4.256\times10^{-5}Z_3\theta$$
$$F_{Interaction(y)} = 7.92\times10^{-5}\theta + 3.011\times10^{-5}Z_1\theta + 3.553\times10^{-5}Z_2\theta + 3.555\times10^{-5}Z_3\theta \quad (26)$$
$$M_{Interaction} = 2.203\times10^{-5} - 5.744\times10^{-5}\theta + 8.041\times10^{-5}Z_1 + 7.586\times10^{-5}Z_2 + 7.476\times10^{-5}Z_3 - 5.932\times10^{-6}Z_1\theta + 6.792\times10^{-6}Z_3\theta$$

Z1 =1 , Z2 = 0 , Z3 = 0	if t/c = 0.15
Z2 =1 , Z1 = 0 , Z3 = 0	if t/c = 0.18
Z3 =1 , Z1 = 0 , Z2 = 0	if t/c = 0.20

Using the superposition principle and obtaining the total force of an appended AUV by adding the bare hull forces and moment with the forces and moment of an appendage without considering the interaction effect of the hull and appendage leads to erroneous results. The error of neglecting the interaction effects is given in Fig. 25 at different drift angle for hydroplane NACA0015.

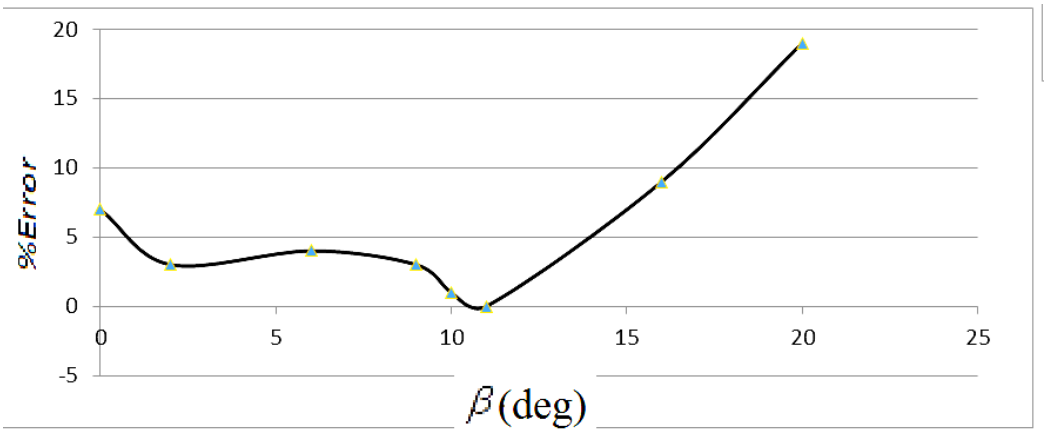

Fig. 25 The error of neglecting the interaction forces at different drift angle for hydroplane NACA0015

Conclusion

Maneuverability is an important hydrodynamic quality of a marine underwater vehicle. The maneuvering characteristics of a marine vehicle should be predicted during the various design stages. There are various models to predict the maneuvering properties of a marine underwater vehicle and among them the Abkowitz model is used more than the others. In this model, the external forces and moments are defined using hydrodynamic derivatives or coefficients based on Taylor series expansion. These hydrodynamic coefficients should be found in advance to predict the maneuvering properties of a marine underwater vehicle.

CFD is used to find these hydrodynamic coefficients of an AUV by virtual simulating captive maneuvering tests. The OTT test is simulated for different drift angles. The simulations are done using the RANS code STAR-CCM+. Unstructured hexahedral trimmed grids are applied to divide the computational domain into discrete control volume. The realizable $k-\varepsilon$ model with a two layer wall function treatment is used to consider the turbulent effects. Grid convergence is performed for simulations. All computations are done using SIMPLE algorithm for pressure-velocity coupling.

The computations are validated with the experimental tests are done in Isfahan University of Technology towing tank. A model of the AUV and four types of hydroplanes are built and the resistance of the bare hull and the appended hull with the various hydroplanes are measured. The comparisons of the measured resistances and the computational results indicate that the CFD computation are reliable.

Simulation of OTT test is done for wide range of the drift angles to compute the transverse velocity dependent coefficients. All the linear and nonlinear coefficients are obtained using time mean of hydrodynamic forces and moment are calculated by CFD simulations.. The coefficients are obtained by using suitable curve fittings.

The linear and nonlinear transverse velocity dependent damping coefficients are affected by the presence of hydroplanes. The linear coefficients Y_v and N_v are affected differently. The coefficient Y_v is increased about 100% by adding the hydroplanes. The effect is almost the same for all kind of hydroplanes and the thickness of the hydroplane has no significant effect. The moment coefficient N_v is highly affected by the position of the hydroplane along the length of the AUV. The hydroplanes are installed at a distance 0.65m from the midship of the AUV. This cause that N_v is decreased by amount of 20% almost in all cases.

The nonlinear coefficient X_{vv} is affected significantly by adding the hydroplane. The effect is more pronounce for NACA0012 and has a minimum effect for NACA0018. It shows that the interaction effect if bare hull and the hydroplane is nonlinear. The nonlinear coefficient Y_{vvv} is increased by about 40% for all cases but the coefficient N_{vv} changes differently. The computation for NACA0012 shows a reduction in N_{vv} and and increment on the other cases. It may be due to the nonlinear interaction between the hull and hydroplane. The interaction between the hull and hydroplanes indicate that the superposition principles cannot be used in computation of the forces and moment for an AUV.

Acknowledgments

The authors gratefully acknowledge the computing time granted by the HPCRC (High Performance Computing Research Center) at Amirkabir University of Technology.

REFERENCES

[1] International Maritime Organization. A: Resolution Standards for Ship Maneuverability. 2002. MSC.137 (76).

[2] International Maritime Organization. B: Explanatory Notes to the Standards for Ship Maneuverability. 2002. MSC/Circ 1053.

[3] Abkowitz M A. Stability and motion control of ocean vehicles. The M.I.T, Cambridge, Massachusetts and London, England. 1969.

[4] Yoshimur Y. Mathematical Model for Maneuvering Ship Motion (MMG Model), Workshop on Mathematical Models for Operations involving Ship-Ship Interaction, Tokyo. 2005.

[5] NomotoK. Analysis of Kempf's Standard Maneuver Test and Proposed Steering Quality Indices, Proceedings of 1st Symposium on Ship Maneuverability, 1960. pp.275- 304.

[6] WilsonR. Paterson E. Stern F. Unsteady RANS CFD method for naval combatants in waves, Proc. 22nd Symp. Naval Hydro. 1998. Washington, D. C.,pp. 532–49.

[7] Gentaz L. Guillerm P E. Alessandrini B. Delhommeau G. Three-dimensional free-surface viscous flow around a ship in forced motion, Proc. 7th Int'l.Conf. Num. Ship Hydro. 1999. Paris, France. pp. 1-12.

[8] Sarkar T. Sayer P G. Fraser S M. A study of autonomous underwater vehicle hull forms using computational fluid dynamics, International Journal for Numerical Methods in Fluids. 1997. Vol 2511, pp. 1301-1313. https://doi.org/10.1002/(SICI)1097-0363(19971215)25:11<1301::AID-FLD612>3.0.CO;2-G.

[9] Nazir Z. Su Y. Wang Z. A CFD Based Investigation of the Unsteady Hydrodynamic Coefficients of 3-D Fins in Viscous Flow. Marine Sci. Apl. 2010. Vol 9 pp. 250-255. https://doi.org/10.1007/s11804-010-1003-8.

[10] Zhang H. Xu Y. Cai H. Using CFD Software to Calculate Hydrodynamic Coefficients, J. Marine Sci. Apl. 2010. Vol 9. pp. 149-155. https://doi.org/10.1007/s11804-010-9009-9.

[11] Tyagi A. Sen D. Calculation of transverse hydrodynamic coefficients using computational fluid dynamic approach. J. Ocean Engineering. 2006. Vol 33, pp.798-809. https://doi.org/10.1016/j.oceaneng.2005.06.004.

[12] Dantas J L D. de Barros E A. Numerical analysis of control surface effects on AUV manoeuvrability, J. Applied Ocean Research. 2013. Vol 42. pp. 168–181. https://doi.org/10.1016/j.apor.2013.06.002.

[13] Ray A. Singh S N. Seshadri V. Evaluation of linear and nonlinear hydrodynamic coefficients of underwater vehicles using CFD, Proceedings of the ASME 28th International Conference on Ocean, Offshore and Arctic Engineering. 2009. https://doi.org/10.1115/omae2009-79374.

[14] Jagadeesh O P, Murali K, Idichandy V G. Experimental investigation of hydrodynamic force coefficients over AUV hull form. Ocean Engineering, 2009, Vol 36, , pp 113-118. https://doi.org/10.1016/j.oceaneng.2008.11.008.

[15] Phillips A, , Turnock S R., and Furlong M. Influence of turbulence closure models on the vortical flow field around a submarine body undergoing steady drift. Journal of marine science and technology. 2010, Vol 15, pp. 201-217. https://doi.org/10.1007/s00773-010-0090-1.

[16] Ferziger H J. Peric M. Computational Methods for Fluid Dynamics. 3th ed. Berlin: Springer; 2002. https://doi.org/10.1007/978-3-642-56026-2.

[17] Shih, T., Liou, W., Shabbir, A., Yang, Z. and Zhu, J.. A new k-epsilon eddy viscosity model for high Reynolds number turbulent flows: Model development and validation. NASA STI/Recon Technical Report N, 95 1994, p. 11442.

[18] Roache P J. Quantification of uncertainty in computational fluid dynamics. Annual Review of Fluid Mechanics. 1997. Vol 29.pp 123-160. https://doi.org/10.1146/annurev.fluid.29.1.123.

Submitted: 02.03.2015.
Accepted: 13.01.2016.

Ahmad Hajivand hajivand@aut.ac.ir, S. Hossein Mousavizadegan, Mohsen Sadeghian, Manochehr Fadavi
424 Hafez Ave, Tehran, Iran, 15875-4413. +98 (21) 64540